JGR Planets

RESEARCH ARTICLE

10.1029/2020JE006573

Influence of Volatiles on Mass Wasting Processes on Vesta and Ceres

R. Parekh[1,2], K. A. Otto[1], R. Jaumann[2], K. D. Matz[1], T. Roatsch[1], E. Kersten[1], S. Elgner[1], and C. Raymond[3]

[1]DLR Institute of Planetary Research, Berlin, Germany, [2]Institute of Geological Science Germany, Freie University of Berlin, Berlin, Germany, [3]Jet Propulsion Laboratory, Pasadena, CA, USA

Key Points:

- We classified and estimated the H/L of mass movements to investigate the mechanisms of deposition on Vesta and Ceres
- Vesta has dry, granular-like slides as dominant mass wasting feature, whereas Ceres has abundant features of flow-like mass movements
- The mass wasting deposit mobility is influenced by the material composition and volatile content on Vesta and Ceres

Supporting Information:

- Supporting Information S1

Correspondence to:

R. Parekh,
rutu.parekh@dlr.de

Citation:

Parekh, R., Otto, K. A., Jaumann, R., Matz, K. D., Roatsch, T., Kersten, E., et al. (2021). Influence of volatiles on mass wasting processes on Vesta and Ceres. *Journal of Geophysical Research: Planets*, *126*, e2020JE006573. https://doi.org/10.1029/2020JE006573

Received 14 JUN 2020
Accepted 18 FEB 2021

Abstract We have analyzed mass wasting features, their distribution and deposit geometry on the two largest main asteroid belt objects—protoplanet Vesta and dwarf planet Ceres—and compared their geomorphology and mobility. Both asteroids have similar surface accelerations, but different surface compositions. Based on our observations and previous studies, we categorized three distinct morphological mass wasting classes: slumps, slides, and flow-like movements. We conclude that Ceres has abundant features of flow-like mass movements. Further, sliding and flow-like characteristics are identified in craters within mid-latitudes which supports the possibility of the presence of water ice in the near subsurface of Ceres. Vesta predominantly shows characteristics of dry granular-like slide features which are distributed homogenously across the surface. By plotting the ratio between fall height (H) and run-out length (L) (effective coefficient of friction, H/L) against the run-out length and spreading width (W), we demonstrate that deposits on Vesta terminate on shorter distances, whereas on Ceres they travel longer distances. The deposit geometry and the similar surface gravity on both asteroids suggest that the material composition and volatile component have a significant effect on deposit emplacement. However, both bodies' mass movements have similar effective coefficients of friction, even though Vesta's regolith is comparatively dry, whereas Ceres is rich in water ice. This leads to the conclusion that volatile content alone cannot be responsible for low effective coefficients of friction, and that more than one geological process is needed to explain the mass motion behavior and morphology.

Plain Language Summary Landslides are one of the most studied geological events on planetary bodies. Many scientists have contributed to a diverse database of knowledge with the aim to better understand these processes. They have been observed for various environmental conditions and are affected by gravity and the physical and chemical composition of the hosting body. However, it is challenging to delineate which specific type or morphology of landslide is sensitive to which parameter. On airless asteroids Vesta and Ceres, landslides have been well preserved, allowing for in-depth analysis using remote sensing data. Interestingly, Vesta and Ceres' substantially different surface compositions have a major effect on landslides, despite their similar gravity. In our study, we have examined and updated the landslide inventory on both bodies, and performed an analysis of deposit mobility which will further enhance our understanding related to the material conditions, their mobility, and surface evolution.

1. Introduction

The Dawn mission was designed to understand the conditions and processes that shaped the formation and evolution of two large planetesimals from the initial stages of planetary accretion (Russell & Raymond, 2011), and was the first mission to visit and orbit two planetary bodies located in main asteroid belt. Both Vesta and Ceres are terrestrial protoplanets with Vesta being a dry rocky body and Ceres a volatile-rich body (Russell & Raymond, 2011). They have provided the opportunity to enhance our understanding of planetary formation related to the existence of volatiles (Buczkowski et al., 2016; Chilton et al., 2019; Combe et al., 2016; De Sanctis et al., 2012, 2013; Jaumann et al., 2012; Sizemore et al., 2019a). As a result of the Gamma Ray and Neutron Detector (GRaND) and Visible and Infrared Mapping Spectrometer (VIR) observations, the connection between the HED meteorites and Vesta has been confirmed. Vesta has experienced significant heating and dehydration (Formisano et al., 2013; Toplis et al., 2013), whereas Ceres appears to be

rich in water ice, which appears to exert control on short-wavelength surface morphology (Otto et al., 2019; Schmidt et al., 2017; Sizemore et al., 2019a, 2019b).

As a result of high-resolution surface images acquired by the Dawn rendezvous mission, Vesta and Ceres have been of particular interest for studies of their surface morphology and geology. The internal and external conditions that shaped the surface of Vesta and Ceres can be studied with the data returned by the mission, including detailed shape models (Preusker et al., 2016) and geological maps (Jaumann et al., 2012; Krohn et al., 2014; Roatsch et al., 2012, 2015, 2016, 2017; Williams, Denevi, et al., 2014). Both Vesta and Ceres have undergone critical erosional processes, including impact cratering, that gradually changed their chemical and physical composition, playing a significant role in their evolution (Russell & Raymond, 2011; Russell et al., 2004, 2012; Toplis et al., 2013). The high-resolution images gathered by the Framing Camera (FC) of the Dawn mission (Sierks et al., 2011) have provided visual evidence of geologic processes including landslides (Otto et al., 2013, 2019; Schmidt et al., 2017; Sizemore et al., 2019a), impact cratering, and huge impact basins (Rheasilvia and Veneneia) on the southern latitudes of Vesta (Marchi et al., 2012; Otto et al., 2013; Schenk et al., 2012). Similarly, the FC data has also improved our understanding related to cryovolcanic processes (Nathues et al., 2020; Ruesch et al., 2016; Sori et al., 2018), large-scale mass wasting features and the existence of subsurface water ice on Ceres (Bland et al., 2016; Buczkowski et al., 2016; Chilton et al., 2019; Duarte et al., 2019; Reddy et al., 2012; Schmidt et al., 2017; Sizemore et al., 2019a). The VIR instrument also found ammoniated phyllosilicates (De Sanctis et al., 2017) on Ceres which are proposed to be linked to geomorphologic features such as flow-like mass wasting features (Chilton et al., 2019; Otto et al., 2013). Overall, landslides are one of the most prominently studied geological features on Vesta and Ceres because of their ability to expose fresh regolith material (Otto et al., 2013; Schmidt et al., 2017). In fact, mass wasting analyses provided clues of granular-like material behavior on Vesta (Krohn et al., 2014; Otto et al., 2013) and the possible existence of subsurface volatiles that may have triggered lubricated mass wasting processes on Ceres (Schmidt et al., 2017).

On Vesta, the classification of mass wasting features was conducted based on morphological characteristics which include intra-crater mass wasting, flow-like and creep-like features, slumps, slides, and curvilinear features within the Rheasilvia basin (Otto et al., 2013). Considering the varying morphological characteristics throughout the southern latitudes on Vesta, it is thought to be the most geologically active region of the asteroid (Schenk et al., 2012). This region is also rich in ejected materials which cover the original surface of the Rheasilvia and Veneneia basins (Otto et al., 2013; Reddy et al., 2012). Another detailed study of a prominent slumping block at the Matronalia Rupes scarp suggests that forces like friction and cohesion affect slump formation (Krohn et al., 2014). Furthermore, gully formation on Vesta suggests a granular-like brittle regolith (Krohn et al., 2014; Scully et al., 2015; Williams, O'Brien, et al., 2014) with characteristics similar to dry gullies on Mars (Crosta, De Blasio, & Frattini, 2018; Crosta, Frattini, et al., 2018). On Vesta, only very few morphologic features, including pitted terrains (Denevi et al., 2012) and interconnected curvilinear gullies (Scully et al., 2015) suggest the presence of volatiles in the regolith, which may have been delivered via impacts.

Previous investigations of landslides on Ceres focused on morphological appearance and spatial distribution (Chilton et al., 2019; Schmidt et al., 2017). Various flow-like mass movement features were identified and were classified in three categories: deposits with thick frontal lobes, dominating latitudes ≥50° (type 1), deposits with broad sheet-like spreading, traveling on longer distances (type 2), and platy lobate sheets with cuspate toes (type 3) (Schmidt et al., 2017). Most of the landslides were identified proximal to crater rims. The morphology, spatial distribution of mass movements and variation in the geometry of the deposits suggest the presence of subsurface ice on a global scale on Ceres (Schmidt et al., 2017; Sizemore et al., 2017, 2019). In addition, the low effective coefficient of friction, defined as the ratio of the fall height (H) and the run-out length (L) of a mass wasting feature, point toward low shear strength which is attributed to icy material in the upper subsurface of Ceres (Chilton et al., 2019). Recently, Duarte et al. (2019) provided a more detailed investigation of Cerean flows based on intermediate flow features. The morphological characteristics of these flows agree with the previously described classification by Schmidt et al. (2017). However, type 2 flows are prominently identified in relatively shallow craters near the polar regions (Duarte et al., 2019), which supports the hypothesis of a shallow subsurface ice layer in the polar latitudes on Ceres, a conclusion also reached by analysis of GRaND data (Prettyman et al., 2017; Schorghofer, 2008, 2016). This ice layer is

thought to be stable for millions of years (Chilton et al., 2019) because of low surface temperatures (Hayne & Aharonson, 2015) and sublimation rates. Further, an extended study conducted by Hughson et al. (2019) showed that type 3 flows resemble fluidized ejecta and they suggest the presence of an ice-rich subsurface with a low coefficient of friction within upper surface material. In a nutshell, the morphology on Ceres is consistent with the ice-rich composition.

Landslides are also commonly studied geological features on other planetary bodies, such as the icy satellites of Jupiter and Saturn including Iapetus, Rhea (Singer et al., 2012) and Callisto (Moore et al., 1999), Pluto's largest satellite Charon (Beddingfield et al., 2020), Mars (Crosta, De Blasio, & Frattini, 2018; Quantin et al., 2004) and the Moon (Brunetti et al., 2015). Previous studies conducted on Iapetus, Rhea, and Callisto provided quantitative measurements of the effective coefficient of friction and demonstrated that landslides on these planetary bodies exhibit unusual long run-out length. The reduction in friction supports the theory of shear heating within icy surfaces (Singer et al., 2012). On Charon, mixtures of H_2O and ammonia hydrates reduce the melting temperature of the ice, decreasing the internal friction without the necessity of large amounts of energy to melt the ice (Beddingfield et al., 2020). Martian landslides have occurred throughout its history and provide a window into its erosional and environmental evolution (Crosta, Frattini, et al., 2018). On the Moon, landslides, including slumping features, appear as fragmented deposits probably triggered by meteorite impacts and the associated impact shock wave propagation (Scaioni et al., 2017; Xiao et al., 2013).

Landslide run-out length, morphological characteristics (such as hummocky surfaces, brittle deposits, wide alcoves, blocky or lobate frontal margins) and deposit spreading depend on the material and environmental conditions during the time of formation, the presence of ice, water or other volatiles and impurities as well as mass wasting triggering factors (e.g., meteorite impacts and shock wave propagation). Depending on the planetary bodies, the influence of these parameters on landslide formation, appearance, and morphology may vary.

On Ceres, previous investigations of mass movements focused on their flow behavior (Chilton et al., 2019; Combe et al., 2019; Duarte et al., 2019; Schmidt et al., 2017), whereas on Vesta the analysis was limited to the mid-latitudes (Marcia, Calpurnia carter and its neighboring regions) and southern regions (Krohn et al., 2014; Otto et al., 2013, 2016; Williams, Denevi, et al., 2014). Using these investigations as a base, we extend existing findings by classifying and comparing three different types of mass wasting processes under similar gravitational conditions but compositionally different environments as present on Vesta and Ceres. Our aim is to classify landslides based on morphology and highlight the similarities and differences. Next, we quantify the mobility of landslide depositions by estimating the effective coefficient of friction and the spreading efficiency on Vesta and Ceres. Our interpretation is based on the analysis of morphological characteristics and geometrical estimations to constrain the effect of volatiles on the morphology of Vesta and Ceres.

2. Data

To identify mass movement features on Vesta and Ceres, we used mosaics of the Low Altitude Mapping Orbit (LAMO) and High-Altitude Mapping Orbit (HAMO) (Roatsch et al., 2012, 2016, 2017) of the Dawn mission's framing camera (Sierks et al., 2011). The Dawn HAMO mosaics have a spatial resolution of ~70 m/pixel for Vesta and 140 m/pixel for Ceres and LAMO mosaics have a spatial resolution of ~20 m/pixel for Vesta and ~35 m/pixel for Ceres (Roatsch et al., 2012, 2015, 2016, 2017). For regions largely shadowed in the mosaics (e.g., the northern hemisphere of Vesta and the polar regions on Ceres), we additionally used individual images (where available) for identification of mass wasting features. Unfortunately, the northern regions of Vesta (≥60°N) were mainly in shadow because of the northern winter during the LAMO phase of Dawn and thus, we had to exclude this particular region in our analysis. The measurements of drop height (H), run-out length (L) and spreading width (W) of deposits was carried out by taking surface profiles using digital terrain model (DTM) mosaics with ~135 m/pixel resolution (with ~10 m vertical accuracy) on Ceres and 92 m/pixel resolution (with ~5 m vertical accuracy) on Vesta (Preusker et al., 2016), derived from stereo pairs. All data used in this work on Vesta and Ceres can be downloaded from the Planetary Data System (PDS) at https://sbn.psi.edu/pds/resource/dawn/dwnvfcL1.html and https://sbn.psi.edu/pds/resource/dawn/dwncfcL1.html, respectively.

Table 1
Key Indicators Are Considered for the Identification and Classification of Mass Movements

Characteristics	Slump	Slide	Flow
Deformation during wasting process	Very little	Yes	Yes
Exposed scar	Partly exposed	Yes	Covered
Transverse features/striations	Possible, but not observed on Vesta and Ceres	No	Yes
Lobate trunks	No	Possible but rare	Yes
Sheet-like wide fans	No	No	Yes
Boulders and spur/gullies	Rare	Common	Rare
Albedo variations	No	Common	Rare

Note. The indicators were adapted from the classification system developed by Dikau et al. (1996).

3. Materials and Method

3.1. Global Mass Movement Feature Classification, Identification, and Mapping

Our mass movement classification is based on the system developed by Dikau et al. (1996). This method categorizes six different mass movement processes namely; falls, topples, slides, lateral spreads, flows, and complex mechanisms. Each category reveals various modes of morphological features, material properties and surface conditions. For example, falls are found on surfaces with steep slopes, topples are recognized in rocky materials, slides are commonly found within dry granular-like materials, lateral spread is prominent in fine grain materials with shallow topography and flow-like movements are common within water rich surfaces (Varnes, 1978). On Vesta and Ceres, based on morphological indicators (Table 1), three common morphological types were noted: slides associated with granular-like behavior (Otto et al., 2013); a wide spread of unconsolidated material, slumps (or rotational slides) exhibiting transverse ridges at lateral margins on large cohesive blocks of material; and, flow-like movements correlated with lobate tongue-like spreading and/or thin sheet-like (Schmidt et al., 2017) large fans with rippled deposition. Each category shows distinct morphological signatures (Table 1) and using this as an identification tool, we mapped and updated the list of mass movement features on Vesta and Ceres. To understand the behavior of mass wasting processes comprehensively, previously identified landslides (Chilton et al., 2019; Duarte et al., 2019; Krohn et al., 2014; Otto et al., 2013; Schmidt et al., 2017) were also included and are marked accordingly in our global maps (Figures 4 and 5).

On Vesta, earlier mapping analyses classified mass wasting features based on geological appearance (Krohn et al., 2014; Otto et al., 2013) in the southern latitudes (30°–60°). These studies either focused on certain regions of the bodies that were of particular interest (e.g., the southern impact basins on Vesta) or concentrated on features of particular interest (e.g., lobate and alcove fan-like flows on Ceres). In our study, the characterization was conducted globally based on multiple morphological impressions of the mass wasting features. To be able to compare the observations on both bodies, we chose the three versatile classes mentioned above (slides, slumps and flow-like movements) (Table 1) which were commonly recognized on both bodies. This classification covers all types of mass wasting features identified at global scale.

In our global mapping campaign on Vesta and Ceres, each of the three mass wasting classes is displayed in a separate color and the symbol geometry is designated to the different mapping surveys. Landslides have been identified and marked by using geomorphological indicators, as listed in Table 1. The mapping was conducted at the scale of 1:125,000 and 1:200,000 in ArcGIS 10.3™ on Vesta and Ceres, respectively, and cataloged in a GIS geodatabase. For a consistent mapping, a fishnet of 150 × 150 m for Vesta and 250 × 250 m for Ceres was evaluated systematically and a minimum feature size of 0.02 and 0.03 km^2 was defined on Vesta and Ceres, respectively.

3.2. Landslide Geometry

One of the most rudimentary methods to estimate the efficiency of landslide deposit mobility is to analyze the effective coefficient of friction represented as the ratio of fall height and run-out length of a mass

wasting feature (H/L) (McEwen, 1989), also known as Heim's ratio (Heim, 1932). The ratio H/L reflects the capacity of material to travel in the direction of movement, whereas the spreading width (W) denotes the material spreading efficiency perpendicular to the direction of motion. Another technique known as center of mass estimation (Cruden, 1980; De Blasio, 2011) uses the center of the scarp and deposit to estimate the values. However, it shows a high level of inaccuracy because of the irregular topography of Vesta and Ceres (Chilton et al., 2019) and thus, we avoided using this method.

To measure the length and width of a landslide, we first identified the boundaries of deposited materials of all possible mass wasting sites. The horizontal run-out length (L) of the deposit was estimated by taking five profiles (evenly distributed within the boundary of the deposit) in the direction of the movement and averaging it. The boundaries at the top of the deposit and the toe of the deposit were considered as starting and end points for these measurements. Similarly, the spread width (W) was estimated by taking five evenly distributed profiles perpendicular to the direction of movement and the average value was considered. Next, the drop height (H) was measured from the top of the scarp to the tip of the deposit (Figure S1). However, in a few regions, because of erosion, the scarp was not clearly identifiable. In such cases, the height of the crater rim or ridge from which the mass wasting feature originated was considered as the highest dropping point. This is common practice for the estimation of vertical fall height when using topography alone (Singer et al., 2012). For each possible landslide site, five profiles were taken for all parameters (H, L, and W).

Out of our marked mass wasting sites, the estimation of all three parameters (H, L, and W) was feasible only for 85 sites on Vesta and 34 on Ceres. The limited number of measurements is because of restrictions in image or DTM resolutions, blurred deposit boundaries or inadequate illumination conditions (e.g., shadowed features), on both bodies. Other than our measurements, we also adapted previous measurements of H and L from Duarte et al. (2019) and Schmidt et al. (2017) of Ceres landslides. After determining the parameters, we compared the material mobility on Vesta and Ceres.

4. Results

The identified mass-wasting features on Vesta and Ceres show significant similarities and differences in terms of geomorphological signatures (Table 2). In this section, we first present details of morphological classes followed by measurements of the deposit geometry.

4.1. Morphological Identification of Landslides on Vesta and Ceres

4.1.1. Slumps (Rotational Slides)

Rotational slides are commonly identified on terrains with extensive slopes and cohesive materials (De Blasio, 2011). A chunk of material detaches from its host surface because of the gravitational pull often triggered via a shock wave propagation (e.g., from a nearby impact) (Shingareva & Kuzmin, 2001), creating a spoon-like circular or semicircular surface of failure (De Blasio, 2011). Cohesion within the sliding mass prevents extensive spreading and the mass maintains most of its original shape along the surface of rupture (Otto et al., 2013), causing a step-like topographic profile with one or multiple scarps (Krohn et al., 2014). At the rest position, the detached material partly exposes the steep surface of rupture and is comparatively flat at the frontal margins. In a few cases, the frontal deposit exhibits transverse ridges or cracks as a result of the material deformation.

Octavia crater (Figure 1a) located at −15.47, 168.48 on Vesta is an examples of a single step rotational slump. The crater is ∼60 km in diameter and ∼9 km deep. The slump head appears on the crater wall with a fall height of ∼4.5 km. The slump deposit covers about 208.9 km^2 of the crater floor. The slump major and minor scarp and the exposed slope are seen in Figures 1a and 1b. The slump block moved downwards from the crown region and the top surface of the detached material leans backwards toward the crater wall. However, even though Octavia's landslide possesses most attributes defining a rotational slide, it appears to have formed in granular material leaving a relatively small head compared with the scarp. Nevertheless, we defined it as slump as it shares predominantly slump attributes. More unambiguous rotational slumps are evident in the basins at the southern latitudes of Vesta including the one on the eastern side of Matronalia Rupes (Krohn et al., 2014) where a huge slumping mass covers approximate 600 km^2 with multiple ridges

Table 2
Summary of Mass Wasting Related Geomorphological Features Identified on Vesta and Ceres

Mass-wasting features	Vesta	Ceres
Slump	Rough, transverse ridges, single and/or multiple heads, located inside craters and along large basin rims	Hummocky, single and/or multiple heads, identified inside large craters
Slide	Overlapping deposits, spur and gullies at crest, boulders on crater floor	Overlapping deposits, spur and gullies, boulders at rim and floor
Flow	Small-scale single frontal lobes, gullies or spur at the rim	Multiple lobate tongues with furrows, thin sheet-like wide fan spreading

and minor scarps. Similar features have also been identified on Ceres, for example, in the crater of Toharu (Figure 1c). The crater is ~150 km in diameter and ~3.5 km in depth, located at −48.32, 155.95. We have identified two slump regions at the western and eastern rim of this crater. The detached slump material slipped along the direction of the slope, exposing a steep scarp. Multiple heads are evident which locally have given rise to subsequent failure, generating multiple steps-like surface features (Figures 1d and 1e). Similar to Vesta, Ceres also has single step slumping features (Figure S2f). Transverse ridges are also evident within some slumping bodies (Figure S2).

Overall, on Vesta and Ceres we noted two types of slump events: (i) slumping areas with multiple deposit blocks and transverse ridges. They are specifically observed within the largest crater on Vesta (e.g., the Rheasilvia crater covering Vesta's southern hemisphere) and within multiple craters on Ceres (Sintana, Toharu, Urvara, Occator, Tupo craters), and (ii) single slumping block features. However, we find handful of candidates which have a single slumping block on both, Vesta (only within Occtavia) and Ceres (at the north west rim of Dantu and within an unnamed crater located at 43.57, 34.94).

4.1.2. Slides

Slides move along a planar shear surface potentially exposing the upper area of the shear surface after coming to a rest (De Blasio, 2011). The foot of the material may undergo disaggregation and the slide material experiences some degree of deformation such as lateral spreading (Otto et al., 2013).

An example of such a slide is seen in Pinaria crater (lat.: −29.54, long.:181.63) on Vesta (Figure 2a). Here, we identify multiple areas of slide material deposition on the crater floor. Slides moved downwards from the crater rim, covering the crater floor and exposing the surface of failure at the northern crater rim. The occurrence and preservation of fragile spur features at the crater rim where the slides originated indicate that Pinaria's slides are relatively young. The slide material traveled on a surface with decreasing slope from 40° to 20°. The process continued until the deposit reached a slope flat enough to hold the material. Similar to Pinaria, an unnamed crater located in the southern part of Ceres (lat.: 22°S, long: 80°W), shows layered piles of slide material on the crater floor (Figure 2b) with spurs and boulders near the crater rim. The boulders' sizes are ≥50 m and indicate that parts of the wasted material are composed of brittle substances.

In general, on both bodies, slide features involve the disintegration and spreading of the sliding material (Figure S3). Usually within this type of mass wasting feature it is challenging to constrain the deposit boundaries as material originating from various crater wall locations often intermix leaving no particular boundary or spreading margins.

4.1.3. Flow-Like Movements

Large-scale flow-like movements occur when the cohesion between individual wasting particles is limited, the particles travel independently within a moving mass (De Blasio, 2011) and material starts behaving like a fluid. Fluidized behavior can be caused by melting of volatiles within the material (Schmidt et al., 2017), saltation (De Blasio, 2011), acoustic fluidization (De Blasio, 2011; Melosh, 1986), or the presence of trapped air bubbles within the material (Shreve, 1966, 1968). While traveling, the moving fragments (granular material and/or other consolidated particles) within the material collide with each other and because of friction, form multiple striations in the direction of travel on the surface. Upon rest, the deposit morphology appears

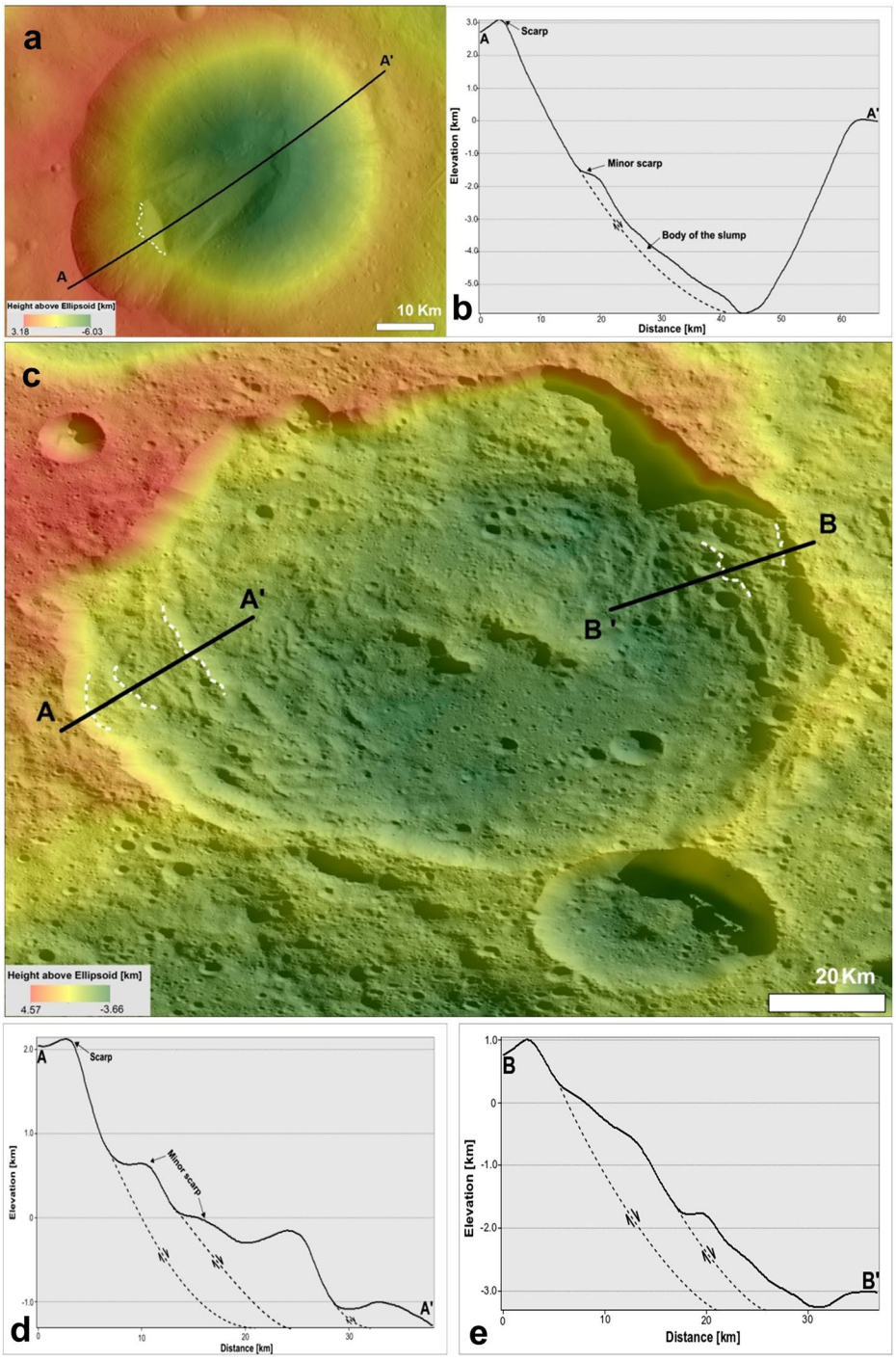

Figure 1. Examples of rotational slumps on Vesta and Ceres. (a) A slump observed in Octavia crater on Vesta with its topographic profile (b). (c) Multiple slump examples observed along Toharu crater's wall on Ceres. The slumps show a step-like profile (in d and e) with multiple minor scarps (white dotted line in c) and deposits covering an area of ~1,000 and ~800 km^2, respectively. There is ~1.1 km elevation difference between the western and eastern rim of the crater. Black dotted lines in the topographic profiles (b, d, e) represent the presumed subsurface of rupture joining the scarp outlined in image (a and c).

either in the form of a thin sheet (Schmidt et al., 2017) or multiple lobate tongues at the motion's front depending on the volume of the mass and its spreading efficiency. The striations are the main morphological difference to the slides and slumps described in the sections above.

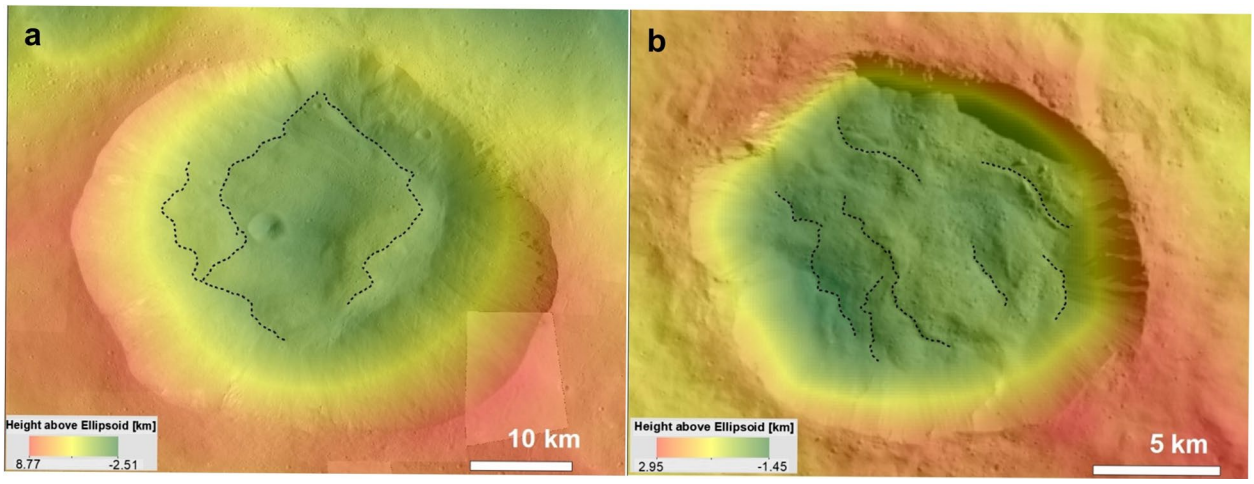

Figure 2. Examples of slides on Vesta and Ceres. Slides emanating from the rim of Pinaria crater on (a) Vesta. (b) Overlapping slide deposits covering an unnamed crater floor on Ceres. Spurs along the crater rim and some larger boulders are evident. The black dotted lines highlight topographic boundaries within the slide material.

On Vesta, for example, a flow-like movement originates from the south east rim of Rufillia crater (~15 km in diameter) and travels toward the crater floor at a slope of ~20° generating two frontal lobes (Figure 3a). The flow-like movement was probably generated by the impact of a younger crater, potentially the one in southeast of the flow feature. The well-preserved morphology of the flow-like feature suggests that it is relatively young. On Ceres, similarly well-defined multiple lobate flow units are evident within and outside of the Haulani crater (Krohn et al., 2017). The units include surface characteristics such as high albedo, fine grained material, multiple flow units, and streak-like or swirled patterns (Krohn et al., 2017). Other than Haulani, there are examples in craters such as Juling, Kupalo, and Urvara (Duarte et al., 2019) also displaying similar mass wasting morphologies (Krohn et al., 2017; Schmidt et al., 2017; Scully et al., 2015). In addition to lobate flow-like features, Ceres also shows prominent impressions of sheet like fans around Xevioso (lat.: 0.7, long.: 310.6) and an unnamed crater (lat.:1.92, long.:309.68), covering ~127 and ~102 km^2 area, respectively, masking the surrounding terrain and suggesting it to be related to impact ejecta (Figure 3b). A detailed analysis of morphological characteristics of ejecta related flows can also be found in Hughson et al. (2019). Fluidized impact ejecta does not necessarily follow the topography (Schmidt et al., 2017) but covers the original landscape. Overall on Ceres flow-like features are generally identified in the regions surrounding craters (Chilton et al., 2019; Combe et al., 2019; Duarte et al., 2019; Hughson et al., 2019; Schmidt et al., 2017).

Usually this type of mass movement travels longer distances than the other two described, suggesting a lower internal friction and/or higher momentum involved in the motion. But there are morphological differences in flow-like movements on both targeted bodies. On Vesta the majority of flow-like features appears as small elongated features with lobate shaped fronts (Figures S4a–S4c), whereas on Ceres a large number of sheet-like features expressed as wide fans with multiple lobes at the flow front (Figures S4d and S4e) are present.

4.2. Global Distribution of Mass Wasting Features on Vesta and Ceres

We identified a large number of mass-wasting features within the vicinity of craters, basin walls or on cliffs. In addition, to the previously identified mass wasting features (29 on Vesta by Krohn et al. [2014]; Otto et al. [2013]), we identified 159 further mass-wasting features out of which 74 are slides, 84 flow-like movements, and 1 slump feature (in total 188 mass wasting features) located at mid-latitudes on Vesta. In addition to our inventory, there are a few more slump blocks distributed frequently within Rheasilvia and Veneneia in the southern region of Vesta (Otto et al., 2013) (Figure 4). The strong elevation difference (up to ~20 km high basin walls) makes these regions most favorable for slumping processes. Overall, slumping

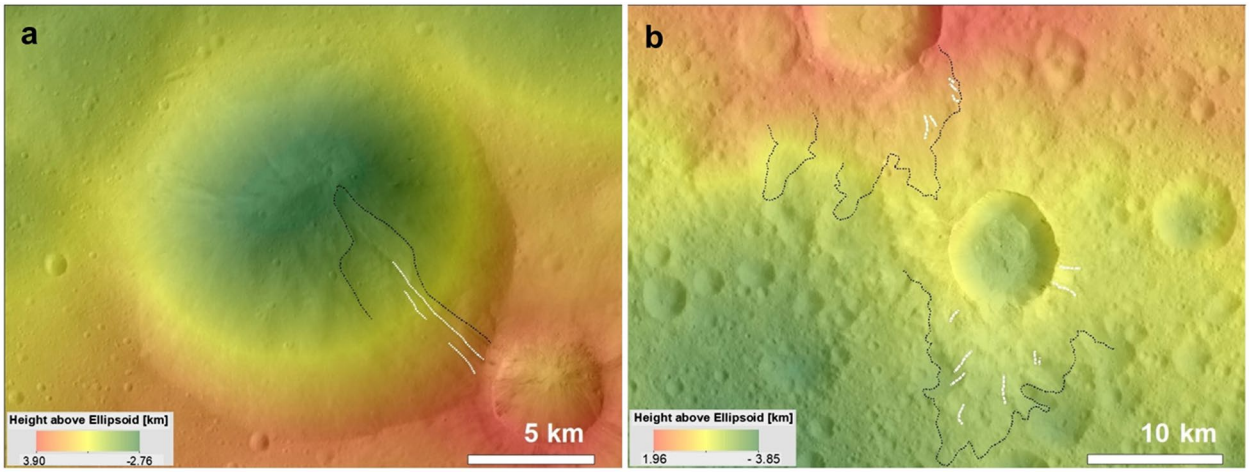

Figure 3. Flow-like movements observed on Vesta and Ceres. (a) A tongue-like flow in Rufillia crater on Vesta and (b) a thin sheet-like flow nearby Xevioso (center crater in which surroundings are highlighted with black dotted lines) and an unnamed (partially visible in the upper center of b) crater on Ceres. The sheet-like flow appearance is common on Ceres and possibly related to ejecta depositions and regolith volatile content (Hughson et al., 2019; Schmidt et al., 2017). The black dotted lines indicate the extent to which material has traveled. The white dotted lines highlight super imposing furrows.

blocks are the largest mass wasting features on Vesta. Nevertheless, the large number of slides on Vesta suggests a prominently dry granular behavior noted at a global scale. Both slides and flow-like movements are correlated with craters of diameters ranging between ~2.6 and 53 km (average of 14.88 km).

On Ceres, previous studies reported 150 mass movement features as flow-like movements (Chilton et al., 2019; Duarte et al., 2019; Schmidt et al., 2017). Besides these, we identified an additional 35 flow-like features, 12 slides and 13 rotational slump (in total 210) features (Figure 5). Flow-like movements are the dominant mass wasting process. Overall, the flow-like mass movements are homogenously distributed on Ceres. However, the other two mass wasting features, slump and sliding features, are not present in Ceres' polar regions and confined within 0°–60° latitude. Further, slides and flow-like impressions are noted in or around craters which have diameters from ~5.1 to ~77.8 km (with an average of 26.5 km). Similar to Vesta, slumping blocks are also present on Ceres within large craters (average size ~61.4 km). Usually the flow-like morphologies are evident within crater floors and along/around crater rims.

4.3. Geomorphologic Measurements

4.3.1. Effective Coefficient of Friction

The friction between the wasting particles has a significant influence on the traveling distance of the material. A common way to describe the friction within a mass movement is to analyze the effective coefficient of friction (H/L). We plot the effective coefficient of friction of the different types of mass wasting features identified on Vesta and Ceres against their run-out length (L) which can be assumed as a proxy for a mass movement's volume (Figure 6). Here, we compare H/L and run-out length (L) and additionally show the drop-height (H), indicated by the size of the data point. In Figure 7, we compare the effective coefficient of friction (H/L) with spreading width (W) on Vesta and Ceres. From Figures 6 and 7, we observe the following trends: (1) the effective coefficient of friction (H/L) of landslides on both Vesta and Ceres follows an approximate linear decrease with run out length (L) in a double logarithmic plot; (2) for a given run-out length, there is no strong relation between run-out length and the friction coefficient on Vesta and Ceres (e.g., a range of values is observed for each value of L); (3) the drop height (H) is lower on Ceres than on Vesta possibly because of the higher topographic relief on Vesta (~40 km elevation difference overall on Vesta compared with 14.5 km on Ceres); and (4) material traveling ≥10 km is more common on Ceres compared with Vesta with the longest travel distance being ~66.4 km on Ceres and ~60.6 km on Vesta, despite Ceres' smaller topographic range. On Vesta the southern hemisphere has a prominent difference in elevation because of the large impact basins Veneneia and Rheasilvia which cause high drop heights for wasting materials.

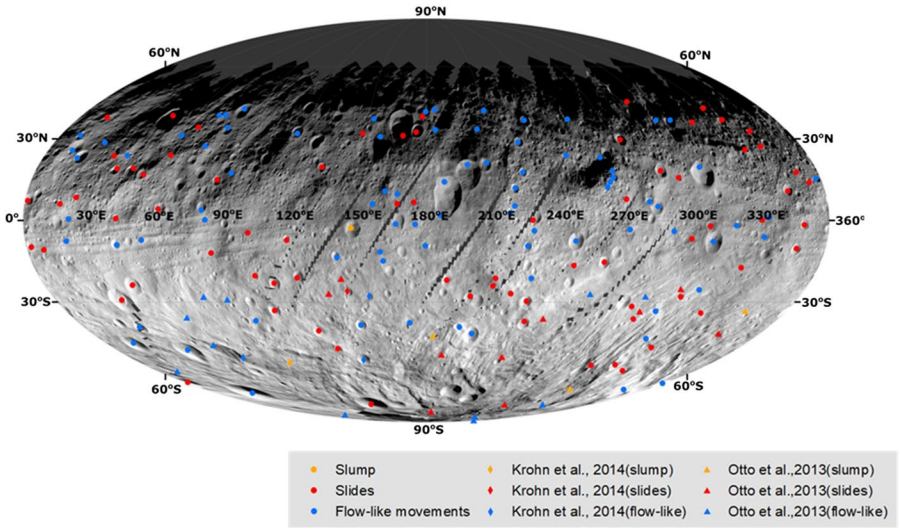

Figure 4. Global distribution of classified mass wasting features on Vesta. For a comprehensive analysis, we have also included and categorized mass wasting features identified by Krohn et al. (2014) and Otto et al. (2013) in the southern region. Additional features found and analyzed in this work are marked as dots. The classification map was prepared using a LAMO mosaic in Mollweide projection.

The range of H/L for each of the three categories on Vesta and Ceres is provided in Table 3. Slides and flow-like movements evenly cover the entire range of measured run-out lengths (L) 0.57–23 km on Vesta (Figure 6). Slumps appear to have larger run-out length (10–60 km) possibly because of their comparatively large size. The slope of the least squares fit of a power function to the data (linear in log-log plot) of each morphological class was estimated. To understand the relation between two parameters (here H/L with L) in quantitative manner we derived the slope of least squares fit. The slope in these diagrams shows how strongly the effective coefficient of friction changes when the run-out length increases. A steep slope means that the effective coefficient of friction decreases with run-out length at a higher rate compared with a less steep slope in these diagrams. This rate of decreasing effective coefficient of friction may hint at the different processes which could also be caused by different materials such as volatiles acting within the moving masses. On Vesta the slope is as follows; slump: -0.69 ± 1.15, slides: -0.40 ± 0.12, and flow-like move-

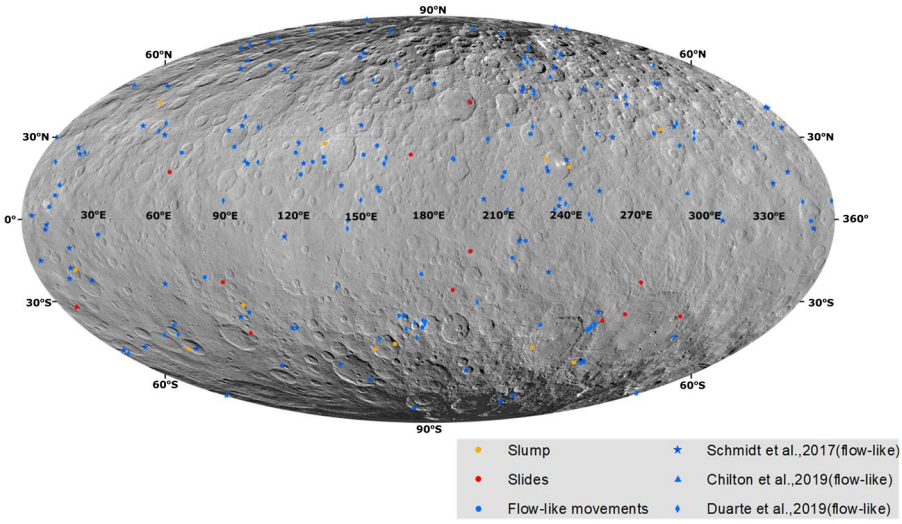

Figure 5. Global distribution of classified mass wasting features on Ceres. In earlier studies, mass wasting features were exclusively classified as flows (Chilton et al., 2019; Duarte et al., 2019; Schmidt et al., 2017). The classification map was prepared using a LAMO mosaic in Mollweide projection.

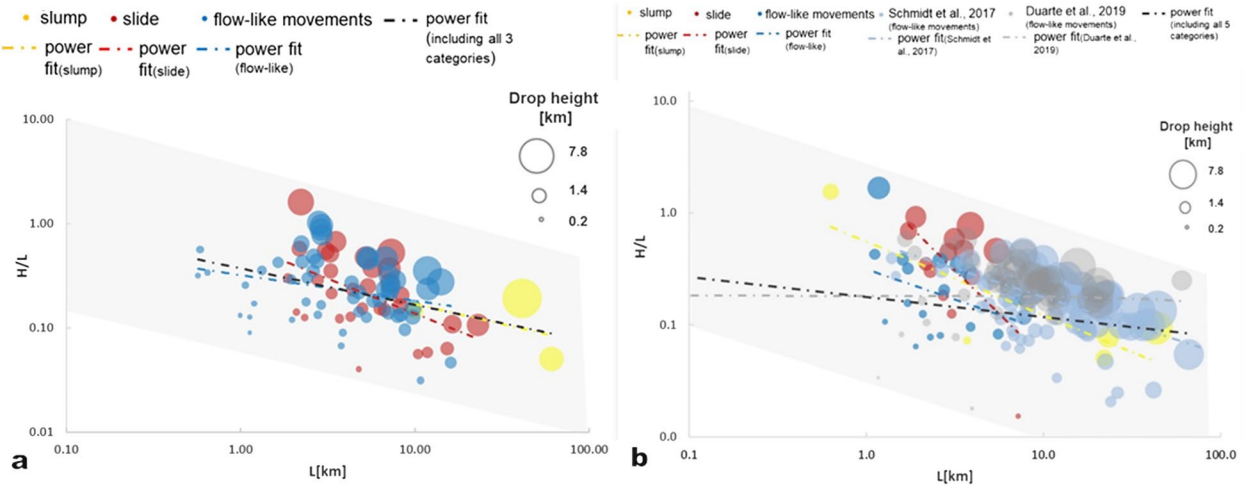

Figure 6. Landslide mobility on (a) Vesta and (b) Ceres. Shown is the measurement of the friction coefficient (H/L) versus the run-out length (L) of the three different types of mass movements. (a) For each category the least squares power law fit between H/L and L yields a slope as follows on Vesta: slump: -0.69 ± 1.15 (yellow dashed-dotted line), slide: -0.40 ± 0.12(red dashed-dotted line), flow-like movements: -0.33 ± 0.15 (blue dashed-dotted line). The combined slope including all types is -0.44 ± 0.11 (black dashed-dotted line). (b) Similarly, the slopes on Ceres are: slump: 0.82 ± 2.80 (yellow dashed-dotted line), slide: -0.22 ± 0.09 (red dashed-dotted line), flow-like movements: -0.08 ± 0.06 (blue dashed-dotted line). In addition to our measurements we also included data from Duarte et al. (2019) and Schmidt et al. (2017). Their slopes are 0.31 ± 0.27 and 0.0 ± 0.14, respectively. On Ceres the slope of H/L versus L for all type of landslides combined is -0.03 ± 0.05. The gray shaded area is to highlight the range of H/L values for a given L and is for orientation only. The size of the dots corresponds to the drop height. x and y axis are in logarithmic scale. Measurements adopted from earlier studies are highlighted in a lighter shade.

ments: -0.33 ± 0.15(Table 3, Figure 6a). All three categories are consistent by having a negative slope which means that the effective friction of coefficient (H/L) tends to decrease with increasing run-out length (L), which can be assumed as a proxy for the mass movement's volume; however, looking at the large error to the fits, the trend is not strong. Likewise, the fitted slope of all types of mass movements on Ceres is as follows; slump: 0.82 ± 2.80, slides: -0.22 ± 0.09, and flow-like moments: -0.08 ± 0.06 (Table 3, Figure 6b). Similar to Vesta, on Ceres slide and flow-like features have negative correlations between their effective coefficient

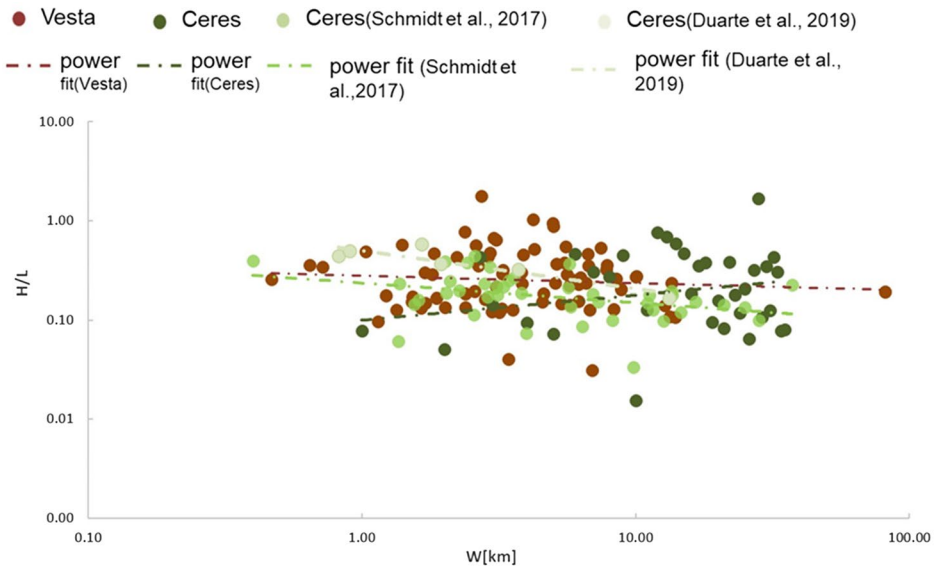

Figure 7. Deposit width versus landslide mobility. Illustrated is the friction coefficient versus the deposit width. Earlier measurements of the friction coefficient (Duarte et al., 2019; Schmidt et al., 2017) are added. The least squares power fit between H/L with W yields slopes as follow: Vesta: -0.10 ± 0.13, Ceres: 0.38 ± 0.21, data from Schmidt et al. (2017): -0.68 ± 0.27 and Duarte et al. (2019): -0.48 ± 0.14. The deposit width was measured from the supporting information provided in the mentioned publications. Note, both axes are in logarithmic scale.

Table 3
Summary of H/L Range and Their Fitted Slope for All Types of Mass Wasting Movements Identified on Vesta and Ceres

	Vesta		Ceres	
Mass-wasting features	H/L range	Fitted slope	H/L range	Fitted slope
Slump	0.05–0.15 (mean 0.13 ± 0.06)	0.69 ± 1.15	0.05–1.54 (mean 0.31 ± 0.59)	0.82 ± 2.80
Slide	0.04–0.61 (mean 0.30 ± 0.29)	−0.40 ± 0.12	0.02–0.92 (mean 0.43 ± 0.25)	−0.22 ± 0.09
Flow	0.03–1.02 (mean 0.30 ± 0.22)	−0.33 ± 0.15	0.06–1.67 (mean 0.13 ± 0.17)	−0.08 ± 0.06

of friction and run-out length. On both planetary bodies, the slumping fit shows a relatively high value of error which may be influenced by the small number of data points. In the case of Mars and Earth, the H/L values range from 0.1 to 0.3 for rock avalanches and 0.01 to 0.1 for saturated terrestrial submarine landslides (Quantin et al., 2004). The slides and flow-like movements on Vesta and Ceres appears less confined and cover a wider range of H/L values. Furthermore, the different gravitational pull and atmospheric condition on the planets and the asteroids makes a direct comparison unreasonable.

There is a prominent distinction between slides and flow-like features in terms of mobility on Ceres; slides terminate at shorter distances (average: ~3.3 ± 0.07 km), whereas flow-like movements have maximum extent up to ~66.4 km (average: ~11.05 ± 10.2 km) on Ceres. This is not observed for Vesta (maximum deposits extend ~16.1 km with average 4.98 ± 3.61 km). However, the range of H/L values is similar on Vesta and Ceres (Vesta: 0.03–1.61, Ceres: 0.02–1.67) regardless of their length.

In addition, we have also analyzed the relationship between the deposit width (W) and friction coefficient (H/L) of mass-wasting features (Figure 7).This provides information about the spreading efficiency of the wasting material perpendicular to the direction of movement. When determining the least squares power fit to the H/L versus W plot in double logarithmic scale, it was observed that for Vesta the slope is −0.10 ± 0.13 and in the case of Ceres the slope is 0.38 ± 0.21, but the correlation is not strong. By plotting the coefficient of friction (H/L) against the width (W) of the deposit, we can demonstrate that mass movement features on Vesta generally do not spread as much as on Ceres, where width up to ~7.5 km on average is commonly measured. This implies that the deposits on Ceres are more mobile in terms of lateral disintegration compared with Vesta. These conditions may be favorable for generating multiple lobate features or sheet like fluidized spreads which are one of the most prominent features on Ceres.

5. Discussion

The global distribution of the identified classes of mass movements illustrates that both Vesta and Ceres have a diverse range of materials at the surface and in their subsurface, resulting in three different mass wasting types. The mass wasting features are present on both bodies but show some similarities (transverse ridges, overlapping slide deposits, boulders and spurs/gullies, brittle material in deposit, lobate tongue-like flow features, single/multiple step like slump, albedo variations) and differences in their morphologies (conglomerate lobate features, hummocky surfaces, sheet-like wide fans). Comparing the global mapping of Vesta and Ceres, slides are the most commonly identified mass wasting type on Vesta, whereas flow-like movements are dominant on Ceres. This is consistent with the fact that Vesta is a dry brittle body (Jaumann et al., 2012) and Ceres is rich in water ice (Prettyman et al., 2017; Schmidt et al., 2017).

5.1. Role of Physical and Chemical Conditions of Surface Material

On Vesta most of the slumping blocks are identified within the southern latitudes (Krohn et al., 2014; Otto et al., 2013). The high elevation difference and steep slope (~40°-10°) (Jaumann et al., 2012) in this region is thought to be favorable for slump formation on Vesta. Slumping behavior is also common within cohesive materials that have the tendency to collapse when reaching a critical abundance of water or has critical slope (angle of repose) on Earth or Mars (Varnes, 1978). Usually a block of slumping material includes cohesive substances like clay, lithic clasts, igneous rocks, organic minerals and materials enriched in water (Varnes, 1978). In the case of Ceres, VIR observations identified carbonates, phyllosilicates and ammoni-

ated clays with OH and/or H_2O mixed within the surface materials possibly explaining the occurrence of slumping on Ceres (Ammannito et al., 2016; Chilton et al., 2019; De Sanctis et al., 2017; Rivkin et al., 2006). Various processes can affect the cohesion between particles of the surface material by weakening bonds. On Ceres, a putative process reducing the material's cohesive strength involves the formation of fracture networks generated either by impact shock wave or from the occasional heating cycle during Ceres' history (Chilton et al., 2019). Most slumping blocks on Ceres are in the mid-latitudes where ice rich materials are possibly present at several meters depth (Bland et al., 2016; Chilton et al., 2019; Prettyman et al., 2017; Schmidt et al., 2017). This may influence the cohesion within the wasting material allowing slumps to occur more frequently in this region. Overall, on Vesta the slumping blocks are correlated with terrain conditions (high altitude, steep slope), whereas on Ceres slumping features are best explained by the surface composition (presence of clays, water ice; Ammannito et al., 2016; Chilton et al., 2019).

Slides are a form of mass movements involving brittle and granular-like behavior. Such materials are common on dry Vesta (Otto et al., 2013) and subsequently they are the most abundant mass wasting features on Vesta. The Vestan mineralogy data collected by visible and infrared spectra shows that the majority of the crust consists of dry eucritic basalts and pyroxene (De Sanctis et al., 2012; Prettyman et al., 2013) which has brittle composition. In the case of Ceres, we have identified craters with granular-like slide behavior near the mid-latitudes. The slide behavior is identified inside craters which have depth from ~0.7 to 1.8 km within ±60° latitude. A possible explanation for the high concentration of slides in the mid-latitudes of Ceres is the lower abundance of water ice within the regolith in these regions (Prettyman et al., 2017). GRaND has detected the ice layer within 1 m of the depth at equator and near to surface at poles on Ceres (Prettyman et al., 2017). The lower ice table depth in the lower latitudes may have caused the upper material layer (which is involved in mass wasting processes) to be drier and thus less cohesive, preferentially generating slides rather than flow-like or slumping features. Thus, distribution of fragmented slides within the mid-latitude points to a relatively brittle ice-rock rich regolith on Ceres, assuming that the depth of the ice layer along with presence of brittle material is the main cause for slides on Ceres, whereas global presence of eucrite and pyroxene dry regolith can be the potential cause for slide on Vesta.

Lastly, on both, Vesta and Ceres, the majority of the flow-like features are located within the vicinity of crater ejecta and/or crater rims. When correlated to impact ejecta, the flow-like features are present at a global scale on both asteroids. Usually, flow-like movements follow the downhill direction however; this movement can sometimes be diverted because of the high mobility of materials affected by the impact. Earlier studies of impact related melt production on Vesta (Williams, O'Brien, et al., 2014) suggest that lobate flows are impact-derived and associated with melt displacement of high velocity impacts (8–10 km/s). Another study finds that the presence of highly shocked and fractured material correlates with the presence of flow-like features within the Rheasilvia basin in the southern hemisphere of Vesta (Otto et al., 2013). Moreover, impact flow movements are also present on much smaller and dry asteroids including (433) Eros (H/L = ~0.03–0.1) (Cheng et al., 2002; Sullivan et al., 2002) and (21) Lutetia (H/L = ~0.4 (Elbeshausen et al., 2012; Massironi et al., 2012). Whereas sheet-like spreading is more commonly identified on Ceres and associated with the presence of water ice in the subsurface (Chilton et al., 2019; Combe et al., 2019; Schmidt et al., 2017). According to GRaND's observations, the presence of shallow subsurface ice (Prettyman et al., 2017) at mid-latitudes and above (~≥50°) correlates with the abundance of flow features (Schmidt et al., 2017). Further, hydrodynamic models suggest low velocity impactors within the asteroid belt (average ~5 km/s velocity; Marchi et al., 2013). At this velocity, impact melts on Vesta may achieve temperatures >1000 K (Marchi et al., 2013) and melt the regolith, whereas on Ceres these impactors may only generate ~300 K which can melt crystalline ice or liberate OH present within the regolith (Bowling et al., 2019; Marchi et al., 2016). Thus, the contrast in the morphology of flow-like mass wasting movements on Vesta and Ceres may be because of the difference in rheology within these two temperature regime. Flow-like mass wasting behavior can be associated with both impact melt and impact-driven mobility as well as post-impact surface temperature and volatile regolith content on Vesta and Ceres.

Both slides and flow-like movements are identified within craters of diameters ranging from ~2.6 to 53 km on Vesta and ~5.1 –77.8 km on Ceres. However, considering their average value (14.9 ± 10.6 km on Vesta and 26.5 ± 23.2 km on Ceres), it is evident that the majority of these features occur within smaller craters which are naturally more abundant (Gou et al., 2018; Hiesinger et al., 2016; Liu et al., 2018) on both asteroid

surfaces. There does not seem to be a correlation between crater size and mass-wasting feature abundance. One thing that is interesting though is that the mass wasting features occur in comparatively larger craters on Ceres than on Vesta. The difference in the size of craters might be because of the fact that (i) large impact craters might have been blanketed by the ejecta of the Rheasilvia and Venetia impact basins (Marchi et al., 2012; Otto et al., 2013; Reddy et al., 2012) and thus are not present on the surface and/or; (ii) because of the lower-resolution LAMO data available for the analysis of Ceres (a factor of ~3 less than on Vesta) that may disguise small-scale features.

5.2. Landslide Effective Coefficient of Friction

The contrast in the morphology of mass movements on Vesta and Ceres may be quantified statistically by comparing properties of landslide mobility. The effective friction coefficient can be correlated to rheological properties. A previous measurement of friction coefficients (Schmidt et al., 2017) suggests similar behavior of Cerean flows to flows on Saturn's icy moon Iapetus. The large range of friction coefficients at a given run-out length is explained by the presence of slippery ice at the surface of motion on Iapetus (Singer et al., 2012). Our investigation shows that a large range of friction coefficients is present on Vesta as well as Ceres (Figure 6). Given that Vesta's regolith is dry, slippery ice theory cannot be the only explanation for a wide range of friction coefficients. Instead, a complex combination of various geological processes is probably involved in planetary mass wasting processes.

To explore the theory of slippery ice on Ceres, we test whether the amount of energy released during the mass movements would be sufficient to create melt. The required energy to melt a kilogram of ice is calculated using the (Turnbull, 2011) equation,

$$E_m = C_p\left(T_f - T_a\right) + \zeta \tag{1}$$

where C_p = specific heat capacity of ice at constant pressure (2.108 kJ/kg/K),

T_f = freezing temperature of ice (273.15 K),

T_a = surface temperature on Ceres (150 K) (Bland et al., 2016), and

ζ = latent heat of fusion (334 kJ/kg) (Turnbull, 2011).

We estimate the specific energy released during the mass movements using the drop height (H = 0.11–4.60 km) and the gravitational force on Ceres (g = 0.27 m/s^2),

$$E_r = gH. \tag{2}$$

This estimate assumes that the entire energy stored in the gravitational potential will be converted into heat and is thus an upper limit to the real values. Our estimations of E_r for all movements on Ceres range between 0.03 and 1.24 kJ/kg. The specific energy required for melting pure ice is ~594 kJ/kg, which is significantly higher than the estimated energy released during mass wasting processes on Ceres. It is therefore unlikely that substantial amounts of ice melted during mass wasting processes on Ceres, however, it is possible that higher temperatures are reached along the landslide bases (Beddingfield et al., 2020). In addition, the presence of carbonates within the material may also reduce the melting temperature of the mixture (Chilton et al., 2019). Thus, the melting of water ice cannot be excluded as possible cause for fluidized movements, but it is probably a minor effect considering the difference in required and provided energy. Nevertheless, note that the above explained calculation does not include the energy released because of the impact. Similar ideas of ice melting cannot be applied to Vesta's flow-like movements as it lacks substantial amounts of volatile materials in the regolith (Jaumann et al., 2012).

We also compared the friction coefficient of mass wasting features of Vesta and Ceres to other icy planetary bodies (Figures 8 and 9). Previous studies (Schmidt et al., 2017; Singer et al., 2012) have compared the effective coefficient of friction of mass wasting flows with Mars and Earth, however, these bodies have significantly larger gravitational acceleration (g). To examine the role of volatiles in the regolith, we compare the H/L range of Vesta and Ceres mass movements with those of planetary bodies of similar g including Iapetus (0.22 m/s^2), Rhea (0.29 m/s^2), and Charon (0.27 m/s^2) in Figure 8. To provide a better visual per-

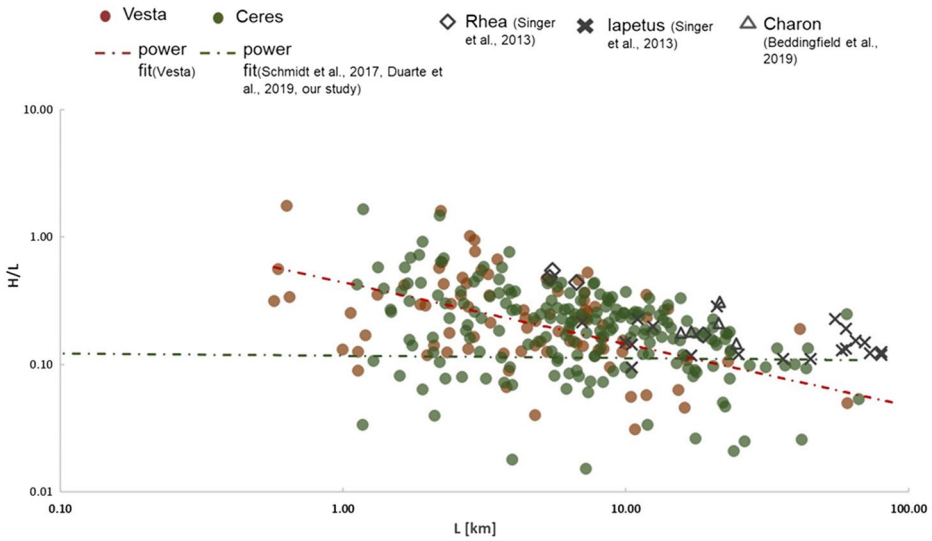

Figure 8. Comparison of landslide mobility on planetary bodies with similar surface accelerations. The identified mass wasting features on Vesta and Ceres are compared with lobate blocky landslides on Iapetus, intra-crater slides on Rhea (Singer et al., 2012), and long run-out slides on Charon (Beddingfield et al., 2020). Small Vesta landslides exhibit similar friction coefficients as the rest of the ice rich planetary bodies. Note that different image resolutions lead to differences in the ranges of measured H and L values.

spective, we have also plotted the data shown in Figure 8 individually for Vesta and Ceres in Figure 9 highlighting each mass wasting category on Vesta and Ceres individually. The icy bodies are much colder than Vesta and Ceres and consist predominantly of volatiles. Even though Vesta is a comparatively dry asteroid, the effective coefficients of friction fall within a similar range as the other icy bodies which have substantial amounts of volatiles and comparatively lower surface temperatures (Figures 8 and 9). We show that flow-like and sliding movements on Vesta have a similar range in H/L values, but are shorter in comparison to landslides on Rhea, Iapetus and Charon (Figure 9). Whereas on Ceres, the flow-like mobility is similar to the other planetary bodies, the slides also terminate at shorter distances. It should be noted that the lower limit of L values of the icy bodies is likely influenced by the generally lower image resolution available for these bodies.

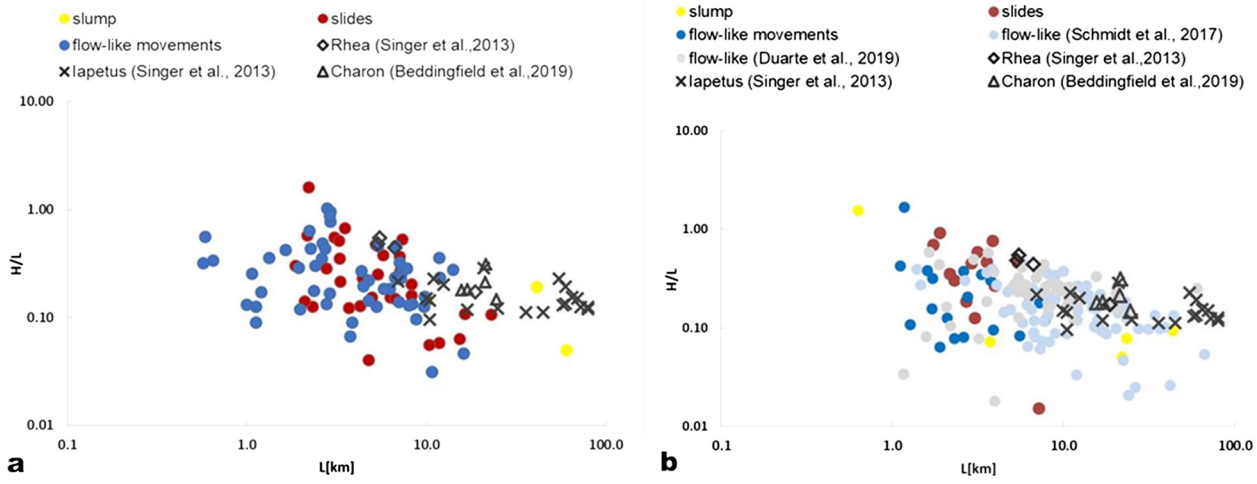

Figure 9. Comparison of landslides classes with other planetary bodies. (a) On Vesta, slides and flow-like movements behave similar to the lobate flows of Iapetus and Charon. However, both the movements on Vesta show shorter run-out lengths. (b) On Ceres, flow-like movements behave similar to the rest of the icy bodies however, slides terminate on shorter distances compared with Iapetus, Rhea, and Charon.

We conclude that the presence of volatiles cannot be the single mechanism in the reduction of the effective coefficient of friction, because we did not observe lower values for the icy bodies and Ceres compared with dry Vesta. Instead, mass wasting measurements follow a common trend with degreasing H/L values for increasing L. Although the low number of landslides detected on some of the icy bodies may bias this observation, the icy bodies appear to have comparatively high H/L values (toward the upper end of the range at a given run-out length). This may hint at the temperature having a more significant influence on landslide mobility than previously thought.

6. Summary

1. We have mapped, analyzed, and classified landslides on Vesta and Ceres to derive a relationship between landslide morphology, coefficient of friction, and mobility. By choosing two bodies with similar surface accelerations, we were able to focus on the regolith volatile content on affecting these parameters.
2. We have identified three common types of mass wasting features on Vesta and Ceres: slumps, slides and fluidized movements. There are some similarities (overlapping deposit pile, transverse ridges, multiple head slumping features, striations, lobate bulges), and differences (abundance of steps like slump deposits, conglomerate lobes, furrows, alcove-like sheets), which we attribute primarily to a varying degree of volatile content on Vesta and Ceres. Further, we also mapped these features at a global scale on both asteroids. In total, the mapping database includes 188 mass wasting features on Vesta and 210 on Ceres.
3. Various types of mass wasting process carved some of distinct geological impressions which have reshaped the surface of Vesta and Ceres. Huge slumps have distorted the crater rims because of collapse of material, and has significant influence on the surface elevation, contributing toward geologically chaotic terrain. Sliding material has produced spur/gully like fragile features at the crater walls and given rise to an albedo dichotomy which can be easily detectable on Vesta even today. Large-scale alcove fan-like deposition has been wrapped in and around cerean craters, concealing the original topography and average slope of the neighboring regions on Ceres.
4. The identified mass wasting features occur on slopes including in or around craters, basin walls or on cliffs. On Vesta, slide and fluidized features are located nearby smaller craters (average 14.8 km), whereas on Ceres the majority of these characteristics are identified within relatively larger crater (average 26.5 km). Slump characteristics are generally associated with larger craters on both bodies. On Ceres, the pole regions do not show any obvious evidence of slumps and slides but they are evident within mid-latitudes, supporting the speculation of vertical variations of ice in the outer shell. Vesta has predominantly dry granular-like slides, whereas on Ceres fluidized mass wasting behavior is dominant.
5. Based on the comparison of run out length (L) and spread width (W) on Vesta and Ceres, we show that mass wasting features on Vesta become immobile on shorter distances and spread less, whereas Cerean mass movements are voluminous, extend up to longer distance and cover larger areas. We suggest that the deposit emplacement is influenced by the difference in impact-induced surface temperature achieved because of contrast in material composition and volatile content. Compared with this, terrain conditions seem to have no significant effect on these values.
6. The effective coefficient of friction varies significantly for a given run-out length or width on both bodies. A general decrease in friction coefficient is observed for larger L values as expected from observations from other planetary mass wasting features. Both bodies have a similar range of friction coefficients (even though Vesta is dry and Ceres is rich in water ice). Thus, the determination of H/L alone may not be sufficient to identify volatile content in mass wasting material. A combined analysis with geomorphologic characteristics is required.
7. Comparing the friction coefficient of Vesta and Ceres with cold ice-rich planetary bodies of similar gravitational acceleration (Iapetus, Charon, and Rhea), we find similar H/L values regardless of the volatile content of the regolith involved and deduce that the temperature, which is much lower on the other ice rich planetary bodies compared with main belt asteroids Vesta and Ceres, may have a more significant influence on H/L on the ice rich planetary bodies than the volatile content.

Data Availability Statement

Image and topographic data used in this work are available at the Small Bodies Node of the Planetary Data System (for link refer Section 2). Derived data products are available via Figshare: R. Parekh (2020) Data for "Influence of Volatiles on Mass Wasting Processes on Vesta and Ceres".7z (https://doi.org/10.6084/m9.figshare.13466642.v1). Measurement results are listed in the supporting information.

Acknowledgments
The authors thank two anonymous reviewers for their constructive and helpful comments that greatly improved this work. The authors acknowledge the Dawn team for providing data and support. The authors extend their gratitude to Chloe Beddingfield and Gou Sheng for sharing their data. The authors are also thankful to Stefan Schröder for helpful discussions. This work was part of the research project "The Physics of Volatile Related Morphologies on Asteroids and Comets". R. Parekh and K. A. Otto gratefully acknowledge the financial support and endorsement from the German Academic Exchange Service (under DLR-DAAD Ph.D. Fellowship) and the DLR Management Board Young Research Group Leader Program by the Executive Board Member for Space Research and Technology. A portion of the work was carried out at the Jet Propulsion Laboratory under contract with NASA.

References

Ammannito, E., DeSanctis, M. C., Ciarniello, M., Frigeri, A., Carrozzo, F. G., Combe, J.-P., et al. (2016). Distribution of phyllosilicates on the surface of Ceres. *Science*, *353*, aaf4279.

Beddingfield, C. B., Beyer, R. A., Singer, K. N., McKinnon, W. B., Runyon, K., Grundy, W., et al. (2020). Landslides on Charon. *Icarus*, *335*, 113383.

Bland, M. T., Raymond, C. A., Schenk, P. M., Fu, R. R., Kneissl, T., Pasckert, J. H., et al. (2016). Composition and structure of the shallow subsurface of Ceres revealed by crater morphology. *Nature Geoscience*, *9*(7), 538–542.

Bowling, T. J., Ciesla, F. J., Davison, T. M., Scully, J. E. C., Castillo-Rogez, J. C., Marchi, S., & Johnson, B. C. (2019). Post-impact thermal structure and cooling timescales of Occator crater on asteroid 1 Ceres. *Icarus*, *20*, 110.

Brunetti, M. T., Xiao, Z., Komatsu, G., Peruccacci, S., & Guzzetti, F. (2015). Large rock slides in impact craters on the Moon and Mercury. *Icarus*, *260*, 289–300.

Buczkowski, D. L., Schmidt, B. E., Williams, D. A., Mest, S. C., Scully, J. E. C., Ermakov, A. I., et al. (2016). The geomorphology of Ceres. *Science*, *353*, aaf4332.

Cheng, A. F., Barnouin-Jha, O., Prockter, L., Zuber, M. T., Neumann, G., Smith, D. E., et al. (2002). Small-scale topography of 433 Eros from laser altimetry and imaging. *Icarus*, *155*, 51.

Chilton, H. T., Schmidt, B. E., Duarte, K., Ferrier, K. L., Hughson, K. H. G., Scully, J. E. C., et al. (2019). Landslides on Ceres: Inferences into ice content and layering in the upper crust. *Journal of Geophysical Research: Planets*, *124*, 1512–1524. https://doi.org/10.1029/2018JE005634

Combe, J.-P., McCord, T. B., Tosi, F., Ammannito, E., Carrozzo, F. G., De Sanctis, M. C., et al. (2016). Detection of local H_2O exposed at the surface of Ceres. *Science*, *353*, aaf3010.

Combe, J.-P., Raponi, A., Tosi, F., De Sanctis, M. C., Carrozzo, F. G., Zambon, F., et al. (2019). Exposed H_2O-rich areas detected on Ceres with the dawn visible and infrared mapping spectrometer. *Icarus*, *318*, 22.

Crosta, G. B., De Blasio, F. V., & Frattini, P. (2018). Introducing a new inventory of large Martian landslides. *Journal of Geophysical Research: Planets*, *5*, 89–119. https://doi.org/10.1002/2017EA000324

Crosta, G. B., Frattini, P., Valbuzzi, E., & De Blasio, F. V. (2018). Global scale analysis of Martian landslide mobility and paleoenvironmental clues. *Journal of Geophysical Research: Planets*, *123*, 872–891. https://doi.org/10.1002/2017JE005398

Cruden, D. M. (1980). The anatomy of landslides. *Canadian Geotechnical Journal*, *17*(2), 295–300.

De Blasio, F. V. (2011). *Introduction to the physics of landslides: Lecture notes on the dynamics of mass wasting*. Springer Science & Business Media.

Denevi, B. W., Blewett, D. T., Buczkowski, D. L., Capaccioni, F., Capria, M. T., De Sanctis, M. C., et al. (2012). Pitted terrain on Vesta and implications for the presence of volatiles. *Science*, *338*(6104), 246–249.

De Sanctis, M. C., Ammannito, E., Capria, M. T., Capaccioni, F., Combe, J.-P., Frigeri, A., et al. (2013). Vesta's mineralogical composition as revealed by the visible and infrared spectrometer on Dawn. *Meteoritics & Planetary Science*, *48*(11), 2166–2184.

De Sanctis, M. C., Ammannito, E., McSween, H. Y., Raponi, A., Marchi, S., Capaccioni, F., et al. (2017). Localized aliphatic organic material on the surface of Ceres. *Science*, *355*(6326), 719–722.

De Sanctis, M. C., Combe, J. P., Ammannito, E., Palomba, E., Longobardo, A., McCord, T. B., et al. (2012). Detection of widespread hydrated materials on Vesta by the Vir Imaging Spectrometer on board the Dawn Mission. *The Astrophysical Journal*, *758*(2), L36.

Dikau, R., Brunsden, D., Schrott, L., & Ibsen, M.-L. (1996). Book review: Landslide recognition: Identification, movement, and causes (21). New York, NY: Wiley and Sons.

Duarte, K. D., Schmidt, B. E., Chilton, H. T., Hughson, K. H. G., Sizemore, H. G., Ferrier, K. L., et al. (2019). Landslides on Ceres: Diversity and geologic context. *Journal of Geophysical Research: Planets*, *124*, 3329–3343. https://doi.org/10.1029/2018JE005673

Elbeshausen, D., Wünnemann, K., Sierks, H., Vincent, J. B., & Oklay, N. (2012). *Landslides triggered by impacts on asteroid (21) Lutetia?* Paper Presented at the European Planetary Science Congress 2012, September 01, 2012.

Formisano, M., Federico, C., Turrini, D., Coradini, A., Capaccioni, F., De Sanctis, M. C., & Pauselli, C. (2013). The heating history of Vesta and the onset of differentiation. *Meteoritics & Planetary Science*, *48*, 2316–2332. https://doi.org/10.1111/maps.12134

Gou, S., Yue, Z., Di, K., & Liu, Z. (2018). A global catalogue of Ceres impact craters ≥ 1 km and preliminary analysis. *Icarus*, *302*, 296.

Hayne, P. O., & Aharonson, O. (2015). Thermal stability of ice on Ceres with rough topography. *Journal of Geophysical Research: Planets*, *120*, 1567–1584. https://doi.org/10.1002/2015JE004887

Heim, A. (1932). *Bergsturz und menschenleben*. Fretz & Wasmuth.

Hiesinger, H., Marchi, S., Schmedemann, N., Schenk, P., Pasckert, J. H., Neesemann, A., et al. (2016). Cratering on Ceres: Implications for its crust and evolution. *Science*, *353*, aaf4758.

Hughson, K. H. G., Russell, C. T., Schmidt, B. E., Chilton, H. T., Sizemore, H. G., Schenk, P. M., & Raymond, C. A. (2019). Fluidized appearing ejecta on Ceres: Implications for the mechanical properties, frictional properties, and composition of its shallow subsurface. *Journal of Geophysical Research: Planets*, *124*, 1819–1839. https://doi.org/10.1029/2018JE005666

Jaumann, R., Williams, D., Buczkowski, D. L., Yingst, R. A., Preusker, F., Hiesinger, H., et al. (2012). Vesta's shape and morphology. *Science*, *336*(6082), 687–690.

Krohn, K., Jaumann, R., Otto, K., Hoogenboom, T., Wagner, R., Buczkowski, D. L., et al. (2014). Mass movement on Vesta at steep scarps and crater rims. *Icarus*, *244*, 120–132.

Krohn, K., Jaumann, R., Otto, K. A., Schulzeck, F., Neesemann, A., Nass, A., et al. (2017). The unique geomorphology and structural geology of the Haulani crater of dwarf planet Ceres as revealed by geological mapping of equatorial quadrangle Ac-6 Haulani. *Icarus*, *316*, 84.

Liu, Z., Yue, Z., Michael, G., Gou, S., Di, K., Sun, S., & Liu, J. (2018). A global database and statistical analyses of (4) Vesta craters. *Icarus*, *311*, 242–257. https://doi.org/10.1016/j.icarus.2018.04.006

Marchi, S., Bottke, W. F., Cohen, B. A., Wünnemann, K., Kring, D. A., McSween, H. Y., et al. (2013). High-velocity collisions from the lunar cataclysm recorded in asteroidal meteorites. *Nature Geoscience*, *6*, 411.
Marchi, S., Ermakov, A. I., Raymond, C. A., Fu, R. R., O'Brien, D. P., Bland, M. T., et al. (2016). The missing large impact craters on Ceres. *Nature Communication*, *7*, 12257.
Marchi, S., McSween, H. Y., O'Brien, D. P., Schenk, P., De Sanctis, M. C., Gaskell, R., et al. (2012). The violent collisional history of asteroid 4 Vesta. *Science*, *336*, 690.
Massironi, M., Marchi, S., Pajola, M., Snodgrass, C., Thomas, N., Tubiana, C., et al. (2012). Geological map and stratigraphy of asteroid 21 Lutetia. *Planetary and Space Science*, *66*(1), 125–136.
McEwen, A. S. (1989). Mobility of large rock avalanches: Evidence from Valles Marineris, Mars. *Geology*, *17*, 1111.
Melosh, H. J. (1986). The physics of very large landslides. *Acta Mechanica*, *64*(1–2), 89–99.
Moore, J. M., Asphaug, E., Morrison, D., Spencer, J. R., Chapman, C. R., Bierhaus, B., et al. (1999). Mass movement and landform degradation on the Icy Galilean Satellites: Results of the Galileo nominal mission. *Icarus*, *140*, 294.
Nathues, A., Schmedemann, N., Thangjam, G., Pasckert, J. H., Mengel, K., Castillo-Rogez, J., et al. (2020). Recent cryovolcanic activity at Occator crater on Ceres. *Nature Astronomy*, *4*, 794.
Otto, K., Jaumann, R., Krohn, K., Matz, K.-D., Preusker, F., Roatsch, T., et al. (2013). Mass-wasting features and processes in Vesta's south polar basin Rheasilvia. *Journal of Geophysical Research: Planets*, *118*, 2279–2294. https://doi.org/10.1002/2013JE004333
Otto, K., Jaumann, R., Krohn, K., Spahn, F., Raymond, C. A., & Russell, C. T. (2016). The Coriolis effect on mass wasting during the Rheasilvia impact on asteroid Vesta. *Geophysical Research Letters*, *43*(24), 12340–12347. https://doi.org/10.1002/2016GL071539
Otto, K., Marchi, S., Trowbridge, A., Melosh, H., & Sizemore, H. (2019). Ceres crater degradation inferred from concentric fracturing. *Journal of Geophysical Research: Planets*, *124*, 1188–1203. https://doi.org/10.1029/2018JE005660
Prettyman, T. H., Mittlefehldt, D. W., Yamashita, N., Beck, A. W., Feldman, W. C., Hendricks, J. S., et al. (2013). Neutron absorption constraints on the composition of 4 Vesta. *Meteoritics & Planetary Science*, *48*, 2211.
Prettyman, T. H., Yamashita, N., Toplis, M. J., McSween, H. Y., Schörghofer, N., Marchi, S., et al. (2017). Extensive water ice within Ceres' aqueously altered regolith: Evidence from nuclear spectroscopy. *Science*, *355*(6320), 55–59.
Preusker, F., Scholten, F., Matz, K.-D., Elgner, S., Jaumann, R., Roatsch, T., et al. (2016). *Dawn at Ceres – Shape model and rotational state*. In Paper Presented at the Lunar and Planetary Science Conference. Retrieved from https://ui.adsabs.harvard.edu/abs/2016LPI....47.1954P
Quantin, C., Allemand, P., & Delacourt, C. (2004). Morphology and geometry of Valles Marineris landslides. *Planetary and Space Science*, *52*(11), 1011–1022.
Reddy, V., Nathues, A., Le Corre, L., Sierks, H., Li, J. Y., Gaskell, R., et al. (2012). Color and albedo heterogeneity of Vesta from Dawn. *Science*, *336*(6082), 700–704.
Rivkin, A. S., Volquardsen, E. L., & Clark, B. E. (2006). The surface composition of Ceres: Discovery of carbonates and iron-rich clays. *Icarus*, *185*(2), 563–567.
Roatsch, T., Kersten, E., Matz, K.-D., Preusker, F., Scholten, F., Elgner, S., et al. (2016). *Dawn FC2 derived Ceres HAMO DTM SPG V1.0. NASA Planetary Data System*. DAWN-A-FC2-5-CERESHAMODTMSPG-V1.0. Retrieved from https://ui.adsabs.harvard.edu/abs/2016PDSS..266.....R
Roatsch, T., Kersten, E., Matz, K.-D., Preusker, F., Scholten, F., Jaumann, R., et al. (2012). High resolution Vesta High Altitude Mapping Orbit (HAMO) Atlas derived from Dawn framing camera images. *Planetary and Space Science*, *73*, 283.
Roatsch, T., Kersten, E., Matz, K.-D., Preusker, F., Scholten, F., Jaumann, R., et al. (2015). Ceres Survey Atlas derived from Dawn Framing Camera images. *Planetary and Space Science*, *121*, 115–120.
Roatsch, T., Kersten, E., Matz, K.-D., Preusker, F., Scholten, F., Jaumann, R., et al. (2017). High-resolution Ceres low altitude mapping Orbit Atlas derived from dawn framing camera images. *Planetary and Space Science*, *140*, 74.
Ruesch, O., Platz, T., Schenk, P., McFadden, L. A., Castillo-Rogez, J. C., Quick, L. C., et al. (2016). Cryovolcanism on Ceres. *Science*, *353*, aaf4286.
Russell, C. T., Coradini, A., Christensen, U., De Sanctis, M. C., Feldman, W. C., Jaumann, R., et al. (2004). Dawn: A journey in space and time. *Planetary and Space Science*, *52*, 465.
Russell, C. T., & Raymond, C. A. (2011). The Dawn Mission to Vesta and Ceres. *Space Science Reviews*, *163*, 3.
Russell, C. T., Raymond, C. A., Coradini, A., McSween, H. Y., Zuber, M. T., Nathues, A., et al. (2012). Dawn at Vesta: Testing the protoplanetary paradigm. *Science*, *336*(6082), 684–686.
Scaioni, M., Yordanov, V., Brunetti, M. T., Melis, M. T., Zinzi, A., Kang, Z., & Giommi, P. (2017). Recognition of landslides in lunar impact craters. *European Journal of Remote Sensing*, *51*(1), 47–61.
Schenk, P., O'Brien, D. P., Marchi, S., Gaskell, R., Preusker, F., Roatsch, T., et al. (2012). The geologically recent giant impact basins at Vesta's South Pole. *Science*, *336*, 694.
Schmidt, B. E., Hughson, K. H. G., Chilton, H. T., Scully, J. E. C., Platz, T., Nathues, A., et al. (2017). Geomorphological evidence for ground ice on dwarf planet Ceres. *Nature Geoscience*, *10*(5), 338–343.
Schorghofer, N. (2008). The lifetime of ice on main belt asteroids. *The Asterophysical Journal*, *682*, 697.
Schorghofer, N. (2016). Predictions of depth-to-ice on asteroids based on an asynchronous model of temperature, impact stirring, and ice loss. *Icarus*, *276*, 88. https://doi.org/10.1016/j.icarus.2016.04.037
Scully, J. E. C., Russell, C. T., Yin, A., Jaumann, R., Carey, E., Castillo-Rogez, J., et al. (2015). Geomorphological evidence for transient water flow on Vesta. *Earth and Planetary Science Letters*, *411*, 151–163.
Shingareva, T. V., & Kuzmin, R. O. (2001). Mass-wasting processes on the surface of phobos. *Solar System Research*, *35*, 431.
Shreve, R. L. (1966). Sherman landslide, Alaska. *Science*, *154*(3757), 1639–1643.
Shreve, R. L. (1968). The Blackhawk Landslide (108). Geological Society of America.
Sierks, H., Keller, H., Jaumann, R., Michalik, H., Behnke, T., Bubenhagen, F., et al. (2011). The Dawn framing camera. *Space Science Reviews*, *163*(1–4), 263–327.
Singer, K. N., McKinnon, W. B., Schenk, P. M., & Moore, J. M. (2012). Massive ice avalanches on Iapetus mobilized by friction reduction during flash heating. *Nature Geoscience*, *5*(8), 574–578.
Sizemore, H., Platz, T., Schorghofer, N., Prettyman, T. H., De Sanctis, M. C., Crown, D. A., et al. (2017). Pitted terrains on (1) Ceres and implications for shallow subsurface volatile distribution. *Geophysical Research Letters*, *44*(13), 6570–6578. https://doi.org/10.1002/2017GL073970
Sizemore, H., Schmidt, B. E., Buczkowski, D. A., Sori, M. M., Castillo-Rogez, J. C., Berman, D. C., et al. (2019a). A global inventory of ice-related morphological features on dwarf planet Ceres: Implications for the evolution and current state of the cryosphere. *Journal of Geophysical Research: Planets*, *124*, 1650–1689. https://doi.org/10.1029/2018JE005699

Sizemore, H., Schmidt, B. E., & Castillo-Rogez, J. (2019b). Introduction to the Special Issue: Ice on Ceres. *Journal of Geophysical Research: Planets*, *124*, 1639–1649. https://doi.org/10.1029/2019JE006012

Sori, M. M., Sizemore, H. G., Byrne, S., Bramson, A. M., Bland, M. T., Stein, N. T., & Russell, C. T. (2018). Author Correction: Cryovolcanic rates on Ceres revealed by topography. *Nature Astronomy*, *2*, 995.

Sullivan, R. J., Thomas, P. C., Murchie, S. L., & Robinson, M. S. (2002). *Asteroid Geology from Galileo and NEAR Shoemaker Data*. In Asteroids III, p. 331.

Toplis, M. J., Mizzon, H., Monnereau, M., Forni, O., McSween, H. Y., Mittlefehldt, D. W., et al. (2013). Chondritic models of 4 Vesta: Implications for geochemical and geophysical properties. *Meteoritics & Planetary Science*, *48*, 2300–2315. https://doi.org/10.1111/maps.12195

Turnbull, B. (2011). Scaling laws for melting ice avalanches. *Physical Review Letters*, *107*, 258001.

Varnes, D. J. (1978). Slope movement types and processes (176).National Academy of Science.

Williams, D., Denevi, B. W., Mittlefehldt, D. W., Mest, S. C., Schenk, P. M., Yingst, R. A., et al. (2014). The geology of the Marcia quadrangle of asteroid Vesta: Assessing the effects of large, young craters. *Icarus*, *244*, 74.

Williams, D., O'Brien, D., Schenk, P., Denevi, B., Carsenty, U., & Marchi, S. (2014). Lobate and flow-like features on asteroid Vesta. *Planetary and Space Science*, *103*, 24–35.

Xiao, Z., Zeng, Z., Ding, N., & Molaro, J. (2013). Mass wasting features on the Moon – How active is the lunar surface? *Earth and Planetary Science Letters*, *376*, 1–11.